Dynamic Characteristics of Railway Subgrade under Heavy Haul Train

Wei Wei
School of Civil Engineering, Central South University, Changsha 410075, China
e-mail:645984212@qq.com

Zeng Zhi-ping
School of Civil Engineering, Central South University, Changsha 410075, China
e-mail:hzzp7475@126.com

Wu Bin
School of Civil Engineering, Central South University, Changsha 410075, China
e-mail: binwu@csu.edu.cn

Wang Wei-dong
School of Civil Engineering, Central South University, Changsha 410075, China
e-mail: 609514588@qq.com

Yan Hai-jian
5th Engineering Company, China Railway 14th Bureau Corporation Limited, Jining, 272117, China
e-mail: 1227517199@qq.com

ABSTRACT

In this paper, the dynamic train model is established by using the multi-body dynamics theory. The track-subgrade dynamic model is established by using the finite element method. The train-track-subgrade dynamic coupling model and the codes are developed with the link of wheel-rail interaction. The distribution of subgrade vibration acceleration and dynamic stress under the axle load of 21t~30t trains at speed of 50 km/h~100 km/h were studied. The results show that: (1) the acceleration and dynamic stress of subgrade increased linearly with the increase of train speed and axle load. (2) The decay rates of acceleration and dynamic stress in the surface of bedding which showed 52% and 43% respectively were the fastest, followed by the underlayer of bedding and subgrade. (3) When the subgrade depth reaches 10 m, the acceleration and dynamic stress of the subgrade do not increase with growth of train speed and axle load. (4) The research results can provide references for the design, construction and maintenance of heavy haul railway subgrade.

KEYWORDS: Heavy haul train; Track; Subgrade; Coupling vibration; Acceleration; Stress.

INTRODUCTION

Subgrade is the basis of railway lines, it should bear the load of superstructure track and the repetition of train load. The superstructure load depends on the type of superstructure, such as ballast track and ballastless track. The train load is a kind of dynamic load, it can be changed with

the axle load, the type of train, the operation speed and direction. Dynamic load is one of the main factors that causing the deterioration of track operating conditions. Excessive dynamic stress of train load will cause the subgrade mud pumping and permanent large deformation of subgrade and resulting in uneven subsidence. Research on dynamic characteristics of Subgrade under train load has been a subject of great importance to many researchers in the world [1-5]. With the increase of train speed, ballastless track has been widely used in high-speed railway [6-10], but the ballasted track is still the main structure of heavy haul railway. For railway subgrade, on the one hand, the train has a dynamic impact on the subgrade structure, which directly affects its working condition and service life. On the other hand, the vibration of subgrade structure has an influence on the stability and safety of the operation train. Therefore, it is necessary to conduct a comprehensive study on the train-track-subgrade interaction. So far, many achievements have been made in the dynamic performance of the train and the track structure [11-13], but the research on dynamic characteristics of subgrade is not deep enough, and the study on train-track-subgrade coupling is far behind the development of heavy-haul railway especially. The existing theoretical analysis and research has been difficult to adapt to the design, construction, maintenance needs of heavy haul railway subgrade. Based on the actual operation situation of heavy haul train, this paper establishes the spatial dynamic analysis model of train-track-subgrade coupling system to explore the dynamic response under different axle load and speed, which can provide reference for the design, construction and maintenance of heavy railway subgrade.

CALCULATION MODEL

The heavy haul train-track-subgrade coupling system is a complex dynamic system, which consists of train subsystem, track subsystem and subgrade subsystem. The subsystem of train, track and subgrade are simulated by different modeling methods for their different construction and vibration characteristics. So the train subsystem is simulated by the multi-rigid-body dynamics method, and the three-dimensional finite element model is used to establish the track-subgrade subsystem. The train subsystem and the track-subgrade system are connected by wheel-rail interaction.

The dynamic model of train subsystem

Figure 1 shows a train consisting of a series of four-wheelset vehicles (rear and front cars numbered 1 and 2, respectively, with N_v trailer cars numbered 1, 2, …, N_v from left to right) moving at a constant speed, v.

Each trailer car of the train is modeled as having a mass-spring-damper system consisting of one car body, two bogies, four wheelsets, and a two-stage suspension system [14]. As shown in Fig.1, the car body rests on the front and rear bogies, each of which is then supported by two wheelsets. The car body is modeled as a rigid body with mass, m_c, and three moments of inertia, I_{cx}, I_{cy}, and I_{cz}. Similarly, each bogie is considered as a rigid body with mass, m_t, and three moments of inertia, I_{tx}, I_{ty}, and I_{tz}. In addition, each wheelset is considered as a rigid body with mass, m_w, and two moments of inertia, I_{wx} and I_{wz}. The secondary suspension between the car body and each bogie is characterized using a three-dimensional system of springs with stiffnesses k_{sx}, k_{sy}, and k_{sz}, and dampers with damping coefficients c_{sx}, c_{sy}, and c_{sz}. Likewise, the springs and shock absorbers in the primary suspension for each wheelset are characterized as k_{px}, k_{py}, and k_{pz}, and c_{px}, c_{py}, and c_{pz}, respectively. By neglecting longitudinal displacements, the motions of the jth trailer car body, with respect to its center of gravity, can be described by X_{cj}, Y_{cj}, Z_{cj}, θ_{cj}, φ_{cj}, and ψ_{cj}. Similarly, the motions of both the rear and front bogies of the jth trailer car can be described,

respectively, by X_{t1j}, Y_{t1j}, Z_{t1j}, θ_{t1j}, φ_{t1j}, and ψ_{t1j} and X_{t2j}, Y_{t2j}, Z_{t2j}, θ_{t2j}, φ_{t2j}, and ψ_{t2j}. Furthermore, the motions from left to right of the hth (h = 1~4) wheelset of the jth trailer car can be described by X_{whj}, Y_{whj}, Z_{whj}, θ_{whj}, and ψ_{whj}, respectively. Therefore, the total number of degrees of freedom (DOFs) for each trailer car is 38.

Each motor car in the train is also modeled as a mass-spring-damper system consisting of a car body, two bogies, four wheelsets, and a two-stage suspension system. The car body has a mass, $m_{Jc,}$ and three moments of inertia, I_{Jcx}, I_{Jcy}, and I_{Jcz}. Each bogie has a mass, m_{Jt}, and three moments of inertia, I_{tx}, I_{ty}, and I_{tz}. Furthermore, each wheelset has a mass, m_{Jw}, and two moments of inertia, I_{Jwx} and I_{Jwz}. The secondary suspension is characterized by springs with stiffnesses k_{Jsx}, k_{Jsy}, and k_{Jsz} and dampers with damping coefficients c_{Jsx}, c_{Jsy}, and c_{Jsz}. The primary suspension is characterized by springs with stiffnesses k_{Jpx}, k_{Jpy}, and k_{Jpz}, and by dampers with damping coefficients c_{Jpx}, c_{Jpy}, and c_{Jpz}. The DOFs of the ith motor car body are denoted as X_{Jci}, Y_{Jci}, Z_{Jci}, θ_{Jci}, φ_{Jci}, and ψ_{Jci}, and the DOFs of both the rear and front bogies of the ith motor car are described, respectively, by X_{Jt1i}, Y_{Jt1i}, Z_{Jt1i}, θ_{Jt1i}, φ_{Jt1i}, and ψ_{Jt1i} and X_{Jt2i}, Y_{Jt2i}, Z_{Jt2i}, θ_{Jt2i}, φ_{Jt2i}, and ψ_{Jt2i}. Furthermore, the motions from left to right of the hth (h = 1~4) wheelset of the ith motor car are denoted as X_{Jwhi}, Y_{Jwhi}, Z_{Jwhi}, θ_{Jwhi}, and ψ_{Jwhi}, respectively.

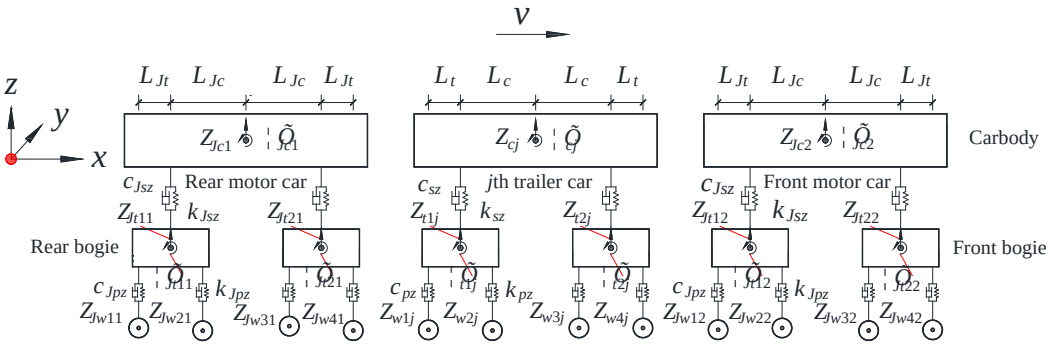

(a) Front view of train

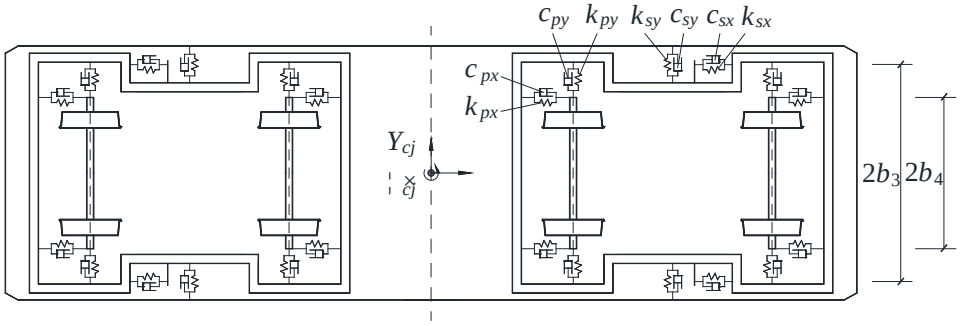

(b) Top view of train

Figure 1: *Continues on the next page*

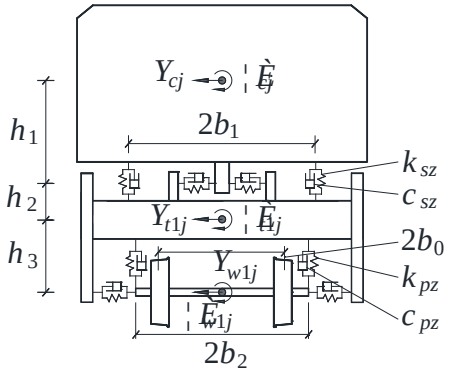

(c) Side view of train

Figure 1: The space vibration analysis model of heavy haul train

The dynamic model of track-subgrade subsystem

Track-subgrade subsystem consists of tracks, fasteners, sleeper, ballast, bedding surface, bedding underlayer, subgrade body and foundation. In this paper, the refinement finite element model of the track-subgrade subsystem is established by using general finite element software to obtaining the mass, stiffness and damping matrix of the subsystem model, and then coupled with the motion equation of the train subsystem. The tracks are simulated by space beam elements. The fasteners are simulated by Spring-damper elements. The solid elements are used to simulate the sleeper, ballast, bedding surface, bedding underlayer, subgrade body and foundation. The dynamic model of subsystem as shown in fig.2. The subgrade body and foundation has been omitted from the figure for clarity.

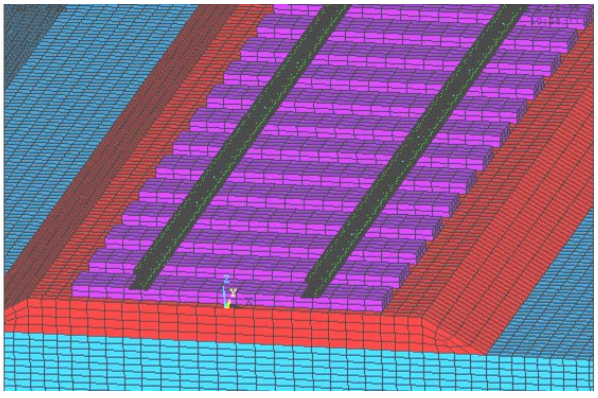

(a) Top view

Figure 2: *Continues on the next page*

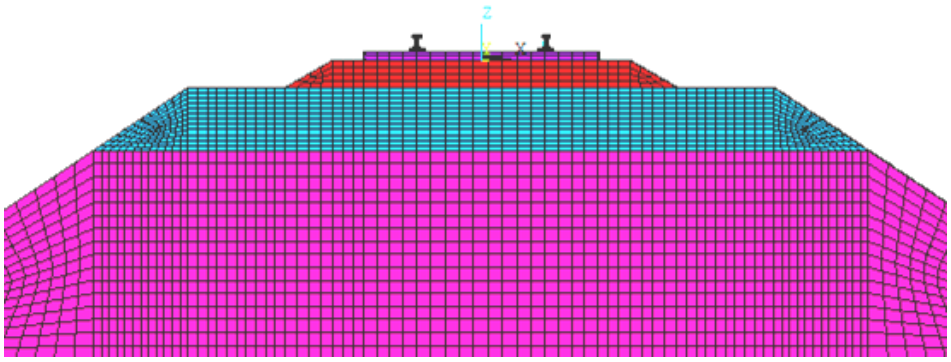

(b) Cross sectional view

Figure 2: The dynamic model of track-subgrade subsystem

The wheel-rail coupling

The coupling of wheel and rail are connected by wheel-rail interaction, as shown in fig.3. The interaction force of wheel and rail mainly includes normal force and creep force. The wheel-rail normal force is calculated according to the Hertz nonlinear elastic contact theory while the wheel-rail creep force is calculated based on Kalker's linear creep theory.

(1) The wheel-rail normal force

On the base of Hertz non-linear elastic contact theory, we derived the wheel-rail normal forces.

$$P(t) = (\frac{1}{G}\Delta Z(t))^{3/2}$$

In the formula, G—constant of wheel-rail contact, $\Delta Z(t)$—Elastic compression between wheel and rail at time t

Elastic compression between wheel and rail, including amount of static compression of wheel can be directly determined by the wheel-rail displacement at the wheel-rail contact point.

$$\Delta Z(t) = Z_{wi} - Z_{ri}(t) \quad (i = 1 \sim 4)$$

In the formula, $Z_{wi}(t)$, $Z_{ri}(t)$—Displacement of the i-th wheel and the rail displacement under it at time t.

When the wheel-rail interface has an irregularity displacement $Z_0(t)$, the expression of wheel rail force is as follow.

$$P(t) = \begin{cases} \left\{ \frac{1}{G}\left[Z_{wi}(t) - Z_{ri}(t) - Z_0(t) \right] \right\}^{3/2} \\ 0 \quad (wheel - rail\ separation) \end{cases}$$

(2) The wheel-rail creep force

Due to the presence of friction, the wheel and rail in the contact patch will produce tangential force, that is, wheel and rail creep force. In this paper, the wheel-rail tangential force is calculated by Kalker's linear theory. In the linear theory of Kalker, it is assumed that the contact areas are all

adhered and the tangential force distribution is symmetrical, so the creep force is linearly related to the creep rate:

$$\begin{cases} F_{xl} = -f_{11}^{l}\xi_{xl} \\ F_{yl} = -f_{22}^{l}\xi_{yl} - f_{23}^{l}\xi_{\psi l} \\ M_{zl} = f_{23}^{l}\xi_{yl} - f_{33}^{l}\xi_{\psi l} \end{cases}$$

$$\begin{cases} F_{xr} = -f_{11}^{r}\xi_{xr} \\ F_{yr} = -f_{22}^{r}\xi_{yr} - f_{23}^{r}\xi_{\psi r} \\ M_{zr} = f_{23}^{r}\xi_{yr} - f_{33}^{r}\xi_{\psi r} \end{cases}$$

In the formula, F_{xl}, F_{yl}, M_{zl} and F_{xr}, F_{yr}, M_{zr} respectively represent left and right force of longitudinal, lateral and spin creep of wheel-rail contact, f_{11} and f_{22} respectively represent longitudinal and lateral creep coefficients, f_{33} represent spin creep coefficient, l and r represent left and right respectively.

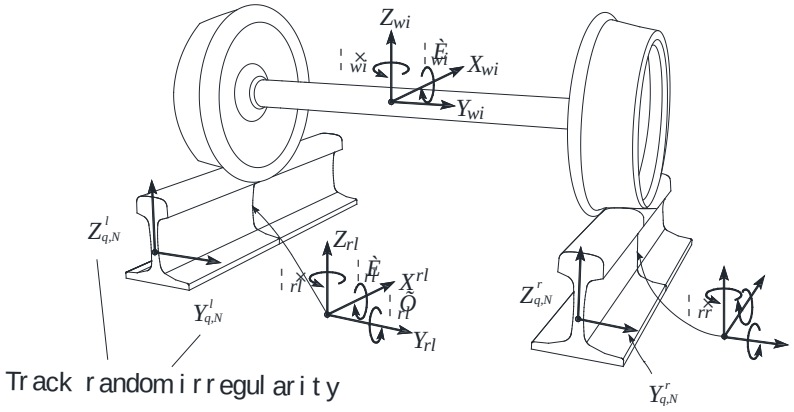

Figure 3: The interaction of wheel and rail

The dynamic analysis program of heavy haul train-track-subgrade system

The thought of heavy haul train-track-subgrade coupling system dynamics analysis program development are as follows:

(1) Compiling the motion equations of train subsystem according to the train subsystem dynamic model.

(2) Obtaining the motion equations of track-subgrade subsystem basing on the dynamic model of the track-subgrade subsystem.

(3) Using the text file to build model data and establish the input and output files in main program, and then read model control parameters, allocate array memory dynamically, read geometric model parameters, material properties parameters and load information from the input files.

(4) Merging the element mass matrix and element stiffness matrix into total mass matrix and total stiffness matrix respectively, obtaining total damping matrix by Rayleigh damping and forming load vector by wheel-rail coupling interaction.

(5) Solving the equations.

The basic calculation flow is shown in fig.4.

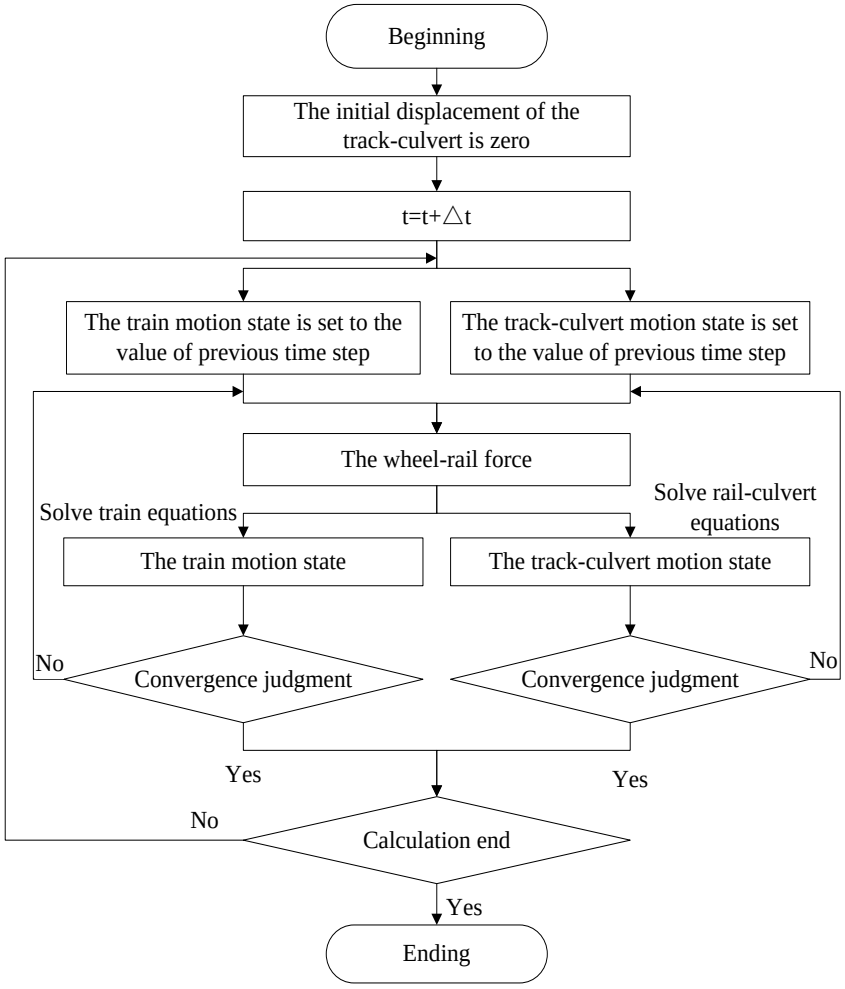

Figure 4: The solution diagram of heavy haul train-track-subgrade coupling dynamic program

ANALYSIS OF DYNAMIC RESPONSE UNDER HEAVY TRAIN LOAD

The calculation parameters

Heavy haul train consist of 8 sections, with axle load of 23t, 25t, 27t and 30t respectively. The main dimension parameters are shown in table1. Track-subgrade structure consists of tracks, fasteners, sleeper, ballast, bedding surface, bedding underlayer, subgrade body and foundation. The calculation parameters of each part are shown in table2. The samples of track random

irregularity randomly generated according to American Class 6 track irregularity and shortwave irregularity.

Generally, the track irregularity can be regarded as stationary ergodic Gaussian random processes characterized by power spectral density (PSD) function [16]. The PSD OF American Class 6 track irregularities, which has been widely used in the train-track coupling vibration [], is used to simulate the middle to long wavelength (greater than 1 m) random track irregularity in this study. Meanwhile, the PSD of Sato track irregularity [17], which has been widely used in the study of high frequency vibration of track structure, is used to simulate the short wavelength (less than 1 m) random track irregularity in this study.

Table 1: The main dimension of train

Axle load (t)	23	25	27	30
Fixed axle spacing (m)	1.83	1.83	1.86	1.86
Bogie center distance (m)	9.21	8.20	9.21	9.926
Full-length of train (m)	13.976	12.000	13.976	13.650
Mass of per meter (kg/m)	64.51	81.67	75.73	86.15

Table 2: The main parameters of track-subgrade structure

Part	Item	Unit	Value
Rail (75 kg/m)	Elastic modulus	Pa	2.11×10^{11}
	Poisson's ratio	—	0.30
	Cross-sectional area	m^2	96.26×10^{-4}
	Density	kg/m^3	7791
Fastener	Vertical stiffness of fasteners	kN/mm	120
	Horizontal stiffness of fastener	kN/mm	45
	Longitudinal stiffness of fastener	kN/mm	45
	Torsional stiffness of fastener	N·m/rad	1.00×10^{13}
	Fastener spacing	m	0.60
	Vertical stiffness of damping	kN×s/m	80
	Horizontal stiffness of damping	kN×s/m	60
	Longitudinal stiffness of damping	kN×s/m	60
	Torsional stiffness of damping	N×m×s/rad	1.00×10^{5}
Sleeper	Elastic modulus	Pa	3.25×10^{10}

	Poisson's ratio	—	0.20
	Sleeper length	m	2.60
	Sleeper density	kg/m^3	2500
	Average width	m	0.32
Ballast	Elastic modulus	Pa	2.50×10^8
	Poisson's ratio	—	0.27
	Density	kg/m^3	2200
	Thickness	m	0.35
	Slope angle	—	1:1.75
	Width of top layer	m	3.60
Bedding surface	Elastic modulus	Pa	1.60×10^8
	Poisson's ratio	—	0.25
	Density	kg/m^3	2100
	Thickness	m	0.70
	Slope angle	—	1:1.5
	Width of top layer	—	8.10
Bedding underlayer	Elastic modulus	Pa	0.80×10^8
	Poisson's ratio	—	0.20
	Density	kg/m^3	1900
	Thickness	m	2.30
	Slope angle	—	1:1.5
Subgrade body	Elastic modulus	Pa	0.60×10^8
	Poisson's ratio	—	0.20
	Density	kg/m^3	1800
	Thickness	m	6.00
	Slope angle	—	1:1.5

The analysis of propagation law of dynamic response on subgrade under heavy haul train

Taking the 30t axle load heavy haul train as an example, it is assumed that the train with the speed of 100km/h running on the track-subgrade structure to obtain the dynamic response characteristics of the subgrade. The amplitude of vertical dynamic stress, attenuation law and time-history curves of different depths are shown in table 3, figure 5 and figure 6. The amplitude of vertical acceleration, attenuation law and time-history curves of different depths are shown in table3, fig.7, fig.8. It can be seen that the dynamic stress and acceleration of the subgrade

decrease gradually with the increase of depth. The decay rates of acceleration and dynamic stress in the surface of bedding which showed 52% and 43% respectively were the fastest, followed by the underlayer of bedding and subgrade. Stress and acceleration were attenuated by 32% and 48% in the range of underlayer of bedding with thickness of 2.3m (depth of 0.7 ~ 3.0m) and by 6% and 9% in the range of subgrade body with depth of 3.0m~9.0m. This is because the train load transmitted into the bedding surface through ballast with the form of dynamic waves, and then spread to deeper. So the dynamic stress and acceleration will decay with the deepen of subgrade for the power falling in the process of transmission.

Table 3: The maximum vertical dynamic stress and acceleration on different depth of subgrade

Subgrade depth (m)	Maximum vertical dynamic stress (kPa)	Maximum vertical acceleration (m/s^2)
0.00	62.90	7.2204
0.35	40.07	5.5041
0.70	30.61	4.4050
1.00	25.02	2.8704
1.40	20.47	1.8504
1.80	17.03	1.3052
2.20	14.34	1.0109
2.60	12.31	0.7710
3.00	10.34	0.5843
3.50	9.16	0.3836
4.00	8.34	0.2882
4.50	7.78	0.2176
5.00	7.40	0.1640
5.50	7.21	0.1223
6.00	6.83	0.0981
7.00	6.58	0.0532
8.00	6.43	0.0289
9.00	6.38	0.0121

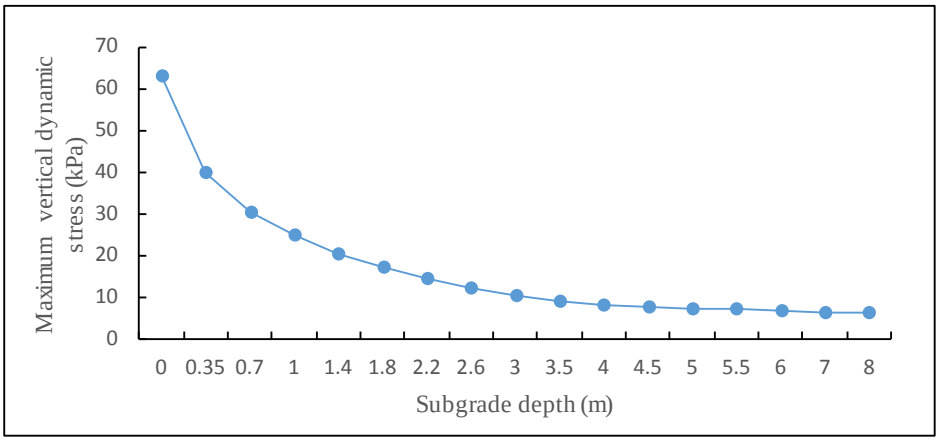

Figure 5: The attenuation law of vertical dynamic stress on depth

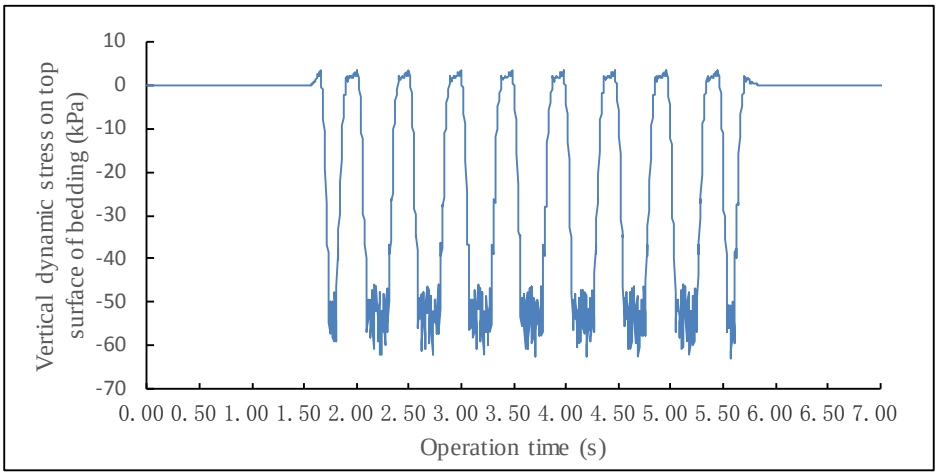

(a) The time-history curve of vertical dynamic stress on top surface of bedding (depth h=0m)

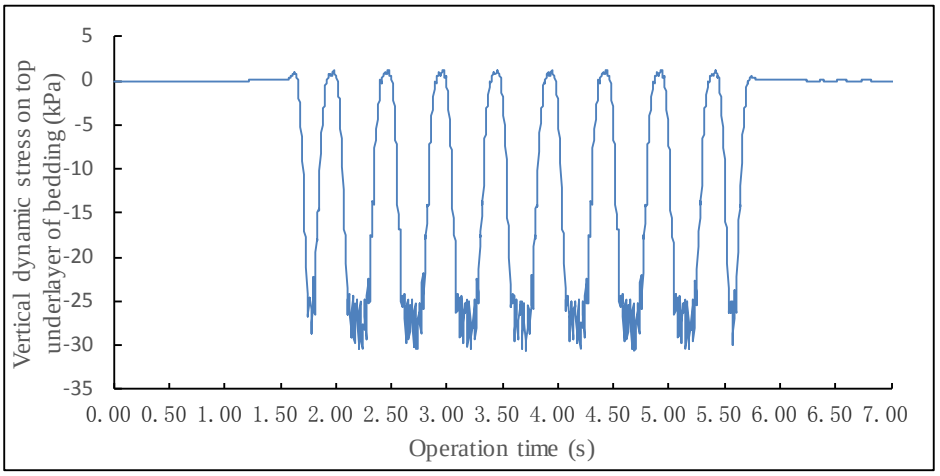

(b) The time-history curve of vertical dynamic stress on top underlayer of bedding (depth h=0.7m)

Figure 6: *Continues on the next page*

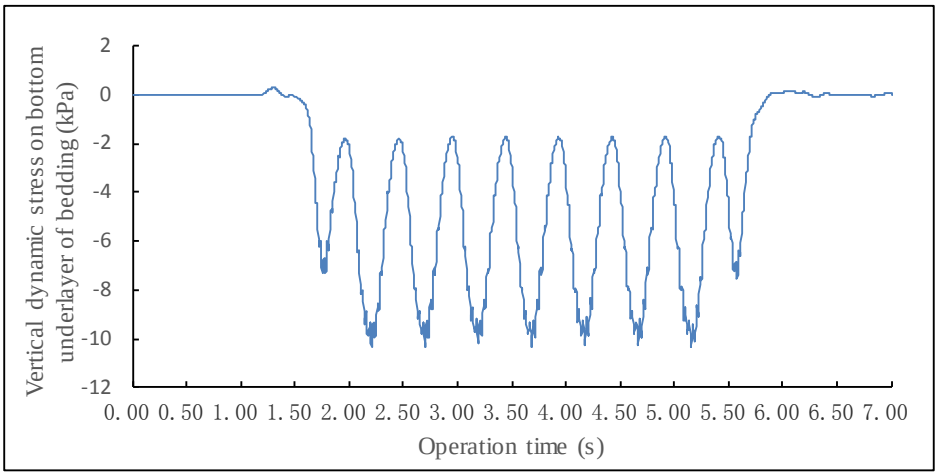

(c) The time-history curve of vertical dynamic stress on bottom underlayer of bedding (depth h=3.0m)

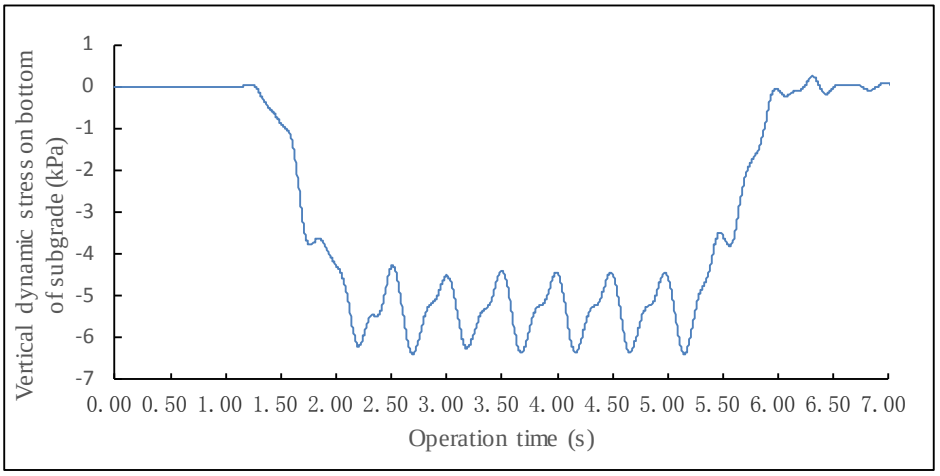

(d) The time-history curve of vertical dynamic stress on bottom of subgrade (depth h=9.0m)

Figure 6: The time-history curve of vertical dynamic stress

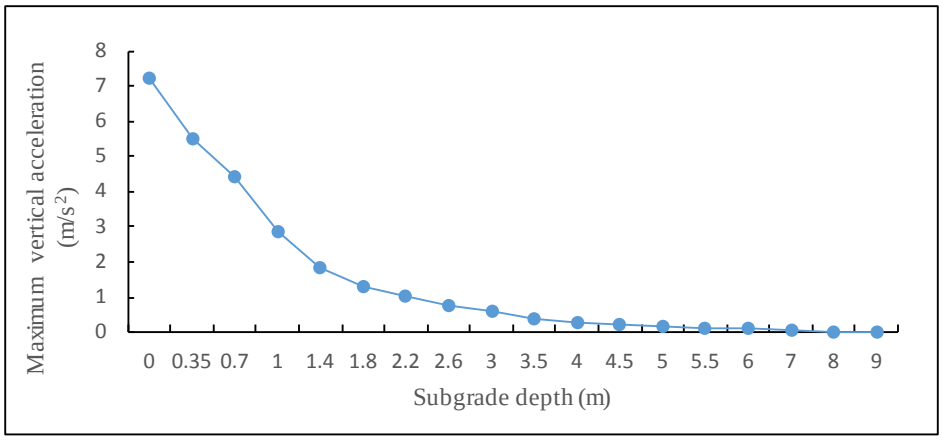

Figure 7: The attenuation law of vertical acceleration on depth

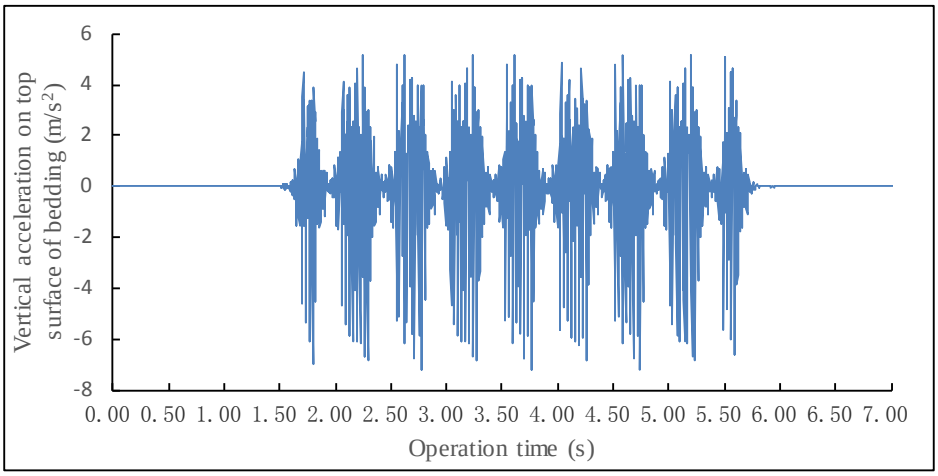

(a) The time-history curve of vertical acceleration on top surface of bedding (depth h=0m)

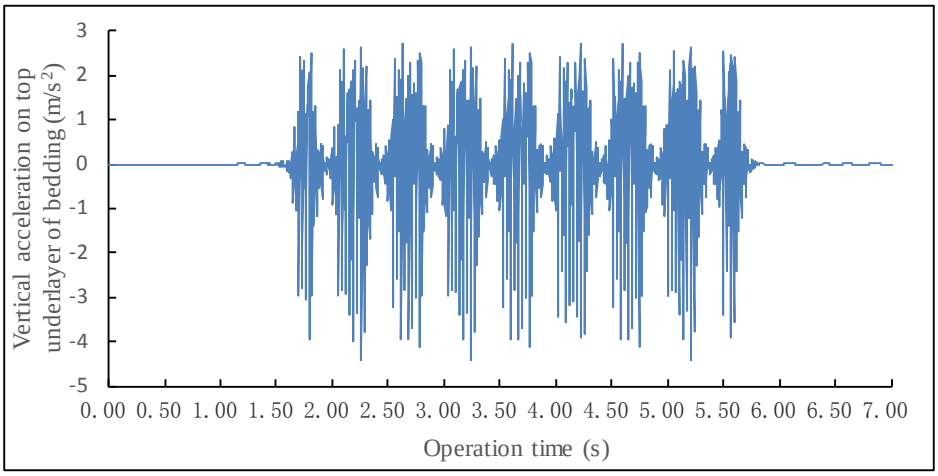

(b) The time-history curve of vertical acceleration on top underlayer of bedding (depth h=0.7m)

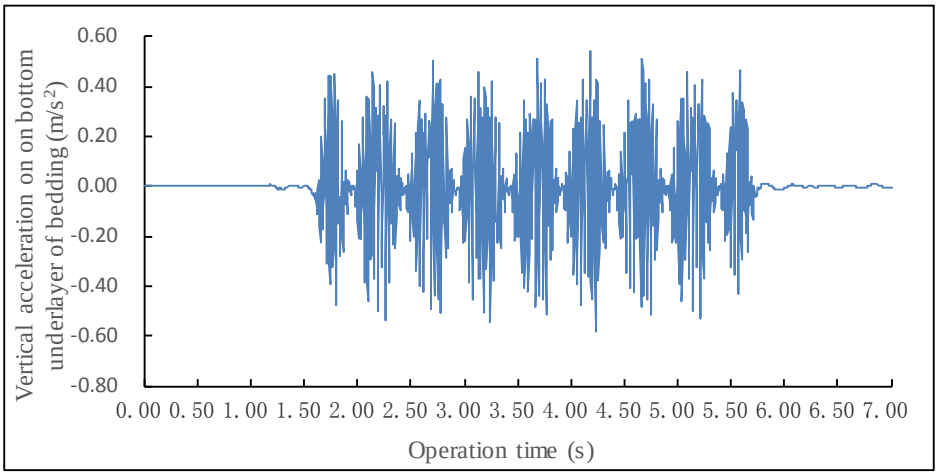

(c) The time-history curve of vertical acceleration on bottom underlayer of bedding (depth h=3.0m)

Figure 8: *Continues on the next page*

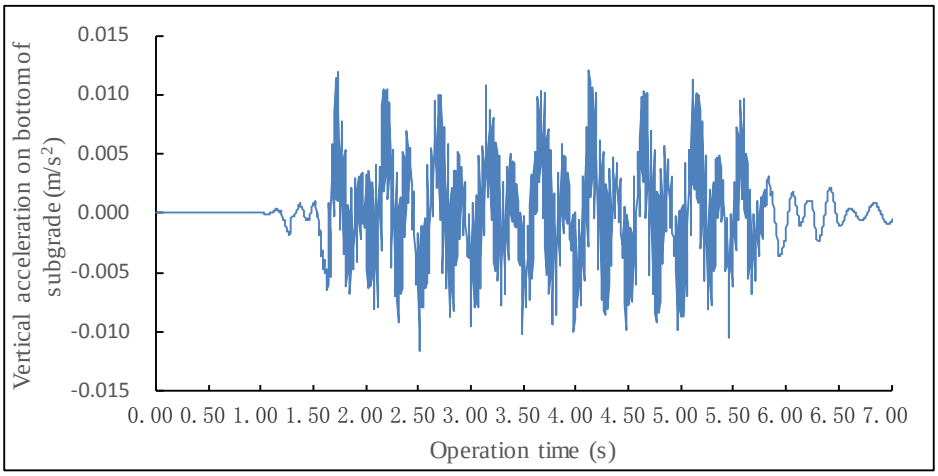

(d) The time-history curve of vertical acceleration on bottom of subgrade (depth h=9.0m)

Figure 8: The time-history curve of vertical acceleration

The analysis of dynamic response of subgrade under train load

The operation speed(v) of the train is 5km/h, 50km/h, 55km/h, 60km/h, 65km/h, 70km/h, 75km/h, 80km/h, 85km/h, 90km/h, 95km/h and 100km/h respectively. Ignoring the track irregularity, the subgrade stress at train speed of 5km/h is used to simulate the static subgrade stress under train load. The results of dynamic response for subgrade under different axle load are shown in table 4 to table 7 and fig.9 to fig.16. The ratio of the subgrade dynamic stress to the subgrade static stress is called the dynamic stress coefficient of subgrade. The dynamic stress coefficients of top surface of bedding under different axle load trains are shown in fig.19 while the dynamic stress coefficients of subgrade in different depth are shown in fig.20.

(1) From the chart, it can be found that the acceleration of subgrade increases with the train speed, but the increase amplitude decreases with the depth. For the 30t axle load train, when the speed increases from 50 km/h to 100km/h, the vertical acceleration top surface of bedding increased from 1.58m/s^2 to 7.22m/s^2, the vertical acceleration top underlayer of bedding increased from 0.90 m/s^2 to 4.41 m/s^2 and the vertical acceleration bottom underlayer of bedding increased from 0.14 m/s^2 to 0.58 m/s^2. When the trains are in the same speed and different axle load, the acceleration of surface bedding and subgrade body increases with the axle load. The acceleration of underlayer bedding is not only related to the axle load, but positively correlated with per meter mass of the train. When the train speed is greater than 90km/h, the vertical acceleration on underlayer of bedding aroused by 25t axle load train is more than the 27t axle load train. When the train speed is 100km/h, the vertical acceleration on underlayer of bedding aroused by 25t axle load train is higher than the 27t axle load train by 8%.

(2) As is shown in the chart, the dynamic stress of subgrade increases with the axle load and train speed. When the train speed is 100km/h, with the axle load rising from 23t to 30t, the dynamic stress of top surface of bedding increased from 47.44kPa to 62.90kPa, the dynamic stress of top underlayer of bedding increased from 22.29kPa to 30.61kPa and the dynamic stress of bottom surface of bedding increased from 6.45kPa to 10.34kPa. In the bedding area, when the axle load rising from 27t to 30t, the average dynamic stress increases is more than 20%. Under the same axle load train, the influence of the growth of train speed on the subgrade dynamic stress decreases with the subgrade depth.

(3) It can be seen that the dynamic stress coefficient of subgrade increases with the growth of train speed, and the influence of the axle load and subgrade depth is not significant on it. For 25t axle load train, when the train speed increased from 50km/h to 100km/h, the dynamic stress coefficient of top surface of bedding grows from 1.036 to 1.231. For 30t axle load train, when the train speed increased from 50km/h to 100km/h, the dynamic stress coefficient of top surface of bedding grows from 1.061 to 1.248. When the 30t axle load train speed is 100km/h, the dynamic stress coefficients are 1.284, 1.258, 1.228, 1.226 and 1.236 respectively while the subgrade depths are 0m, 0.7m, 3.0m, 6.0m and 9m.

Table 4: The dynamic response result of subgrade under 23t axle load train

Calculation index	Operation speed (km/h)						
	5	50	60	70	80	90	100
The vertical acceleration on top surface of bedding (m/s^2)	—	1.4147	1.7977	2.3269	3.3564	4.7980	6.0526
The vertical acceleration on top underlayer of bedding (m/s^2)	—	0.8222	1.2612	1.5897	2.3132	2.9877	3.5205
The vertical acceleration on bottom underlayer of bedding (m/s^2)	—	0.1057	0.1716	0.1900	0.2573	0.3112	0.3726
The vertical acceleration on 6m deep of subgrade (m/s^2)	—	0.0135	0.0228	0.0300	0.0349	0.0429	0.0605
The vertical acceleration on 9m deep of subgrade (m/s^2)	—	0.0023	0.0038	0.0052	0.0053	0.0055	0.0082
The compressive stress on top surface of bedding (m/s^2)	38.54	39.94	40.63	42.79	43.01	44.73	47.44
The compressive stress on top underlayer of bedding (m/s^2)	18.45	18.75	19.18	20.42	20.63	21.18	22.29
The compressive stress on bottom underlayer of bedding (m/s^2)	5.53	5.64	5.82	5.87	5.85	6.17	6.45
The compressive stress on 6m deep of subgrade (m/s^2)	4.08	4.29	4.34	4.19	4.08	4.42	4.43
The compressive stress on 9m deep of subgrade (m/s^2)	3.86	4.11	4.15	4.08	4.02	4.19	4.18

Table 5: The dynamic response result of subgrade under 25t axle load train

Calculation index	Operation speed (km/h)						
	5	50	60	70	80	90	100
The vertical acceleration on top surface of bedding (m/s^2)	—	1.4498	1.8741	2.3715	3.5917	5.1310	6.4043
The vertical acceleration on top underlayer of bedding (m/s^2)	—	0.9174	1.0787	1.4957	2.4908	3.1832	4.1449
The vertical acceleration on bottom underlayer of bedding (m/s^2)	—	0.1011	0.1878	0.2205	0.3597	0.4021	0.4741
The vertical acceleration on 6m deep of subgrade (m/s^2)	—	0.0103	0.0200	0.0271	0.0425	0.0456	0.0648
The vertical acceleration on 9m deep of subgrade (m/s^2)	—	0.0018	0.0034	0.0042	0.0064	0.0064	0.0086
The compressive stress on top surface of bedding (m/s^2)	41.40	42.45	44.08	45.72	46.10	47.87	49.34
The compressive stress on top underlayer of bedding (m/s^2)	20.05	20.56	21.46	21.96	22.10	22.22	23.11
The compressive stress on bottom underlayer of bedding (m/s^2)	6.98	7.11	7.21	7.20	7.20	7.55	7.63
The compressive stress on 6m deep of subgrade (m/s^2)	4.91	4.94	5.04	5.01	5.15	5.28	5.21
The compressive stress on 9m deep of subgrade (m/s^2)	4.73	4.77	4.83	4.86	4.92	4.97	5.06

Table 6: The dynamic response result of subgrade under 27t axle load train

Calculation index	Operation speed (km/h)						
	5	50	60	70	80	90	100
The vertical acceleration on top surface of bedding (m/s^2)	—	1.4727	2.6838	3.1731	4.2685	5.5648	6.8048
The vertical acceleration on top underlayer of bedding (m/s^2)	—	0.8499	1.4003	2.3845	2.7320	3.2703	3.8079
The vertical acceleration on bottom underlayer of bedding (m/s^2)	—	0.1210	0.2058	0.2622	0.2998	0.3970	0.4385

The vertical acceleration on 6m deep of subgrade (m/s^2)	—	0.0167	0.0260	0.0404	0.0447	0.0515	0.0699
The vertical acceleration on 9m deep of subgrade (m/s^2)	—	0.0027	0.0040	0.0071	0.0064	0.0064	0.0087
The compressive stress on top surface of bedding (m/s^2)	43.86	46.03	46.55	48.81	50.21	51.86	52.60
The compressive stress on top underlayer of bedding (m/s^2)	21.09	21.97	22.15	23.51	24.12	24.61	24.91
The compressive stress on bottom underlayer of bedding (m/s^2)	7.21	7.26	7.76	7.83	7.63	7.84	8.31
The compressive stress on 6m deep of subgrade (m/s^2)	5.33	5.51	5.76	5.62	5.35	5.61	5.73
The compressive stress on 9m deep of subgrade (m/s^2)	5.04	5.28	5.48	5.47	5.31	5.36	5.38

Table 7: The dynamic response result of subgrade under 30t axle load train

Calculation index	Operation speed (km/h)						
	5	50	60	70	80	90	100
The vertical acceleration on top surface of bedding (m/s^2)	—	1.5831	2.8612	3.8463	4.7713	5.7274	7.2204
The vertical acceleration on top underlayer of bedding (m/s^2)	—	0.9012	1.5044	2.4304	3.1799	3.9627	4.4050
The vertical acceleration on bottom underlayer of bedding (m/s^2)	—	0.1384	0.2104	0.3816	0.4229	0.4841	0.5843
The vertical acceleration on 6m deep of subgrade (m/s^2)	—	0.0192	0.0262	0.0348	0.0607	0.0768	0.0981
The vertical acceleration on 9m deep of subgrade (m/s^2)	—	0.0030	0.0049	0.0062	0.0102	0.0110	0.0121
The compressive stress on top surface of bedding (m/s^2)	48.98	51.99	56.63	58.14	60.44	61.67	62.90
The compressive stress on top underlayer of bedding (m/s^2)	24.34	26.17	27.39	28.70	29.14	29.35	30.61

The compressive stress on bottom underlayer of bedding (m/s^2)	8.42	8.96	8.93	9.30	9.22	9.79	10.34
The compressive stress on 6m deep of subgrade (m/s^2)	5.57	5.85	5.92	6.18	6.28	6.76	6.83
The compressive stress on 9m deep of subgrade (m/s^2)	5.16	5.43	5.56	5.90	6.25	6.55	6.38

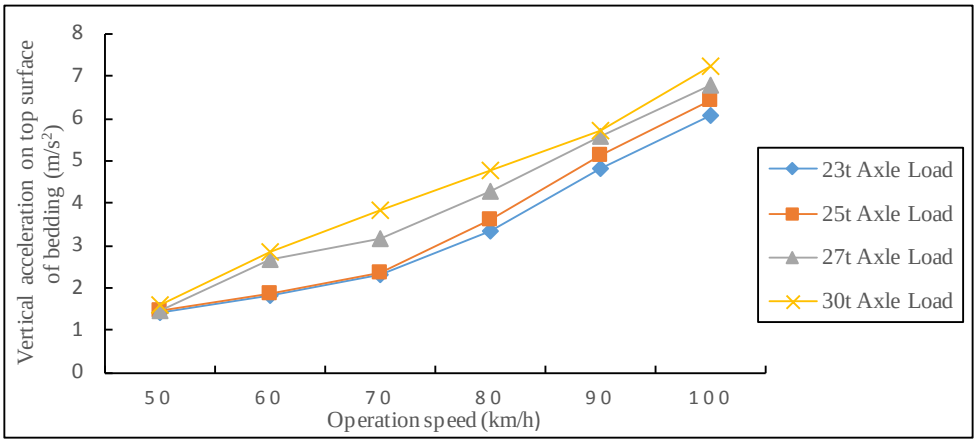

Figure 9: The vertical acceleration on top surface of bedding under different axle load train

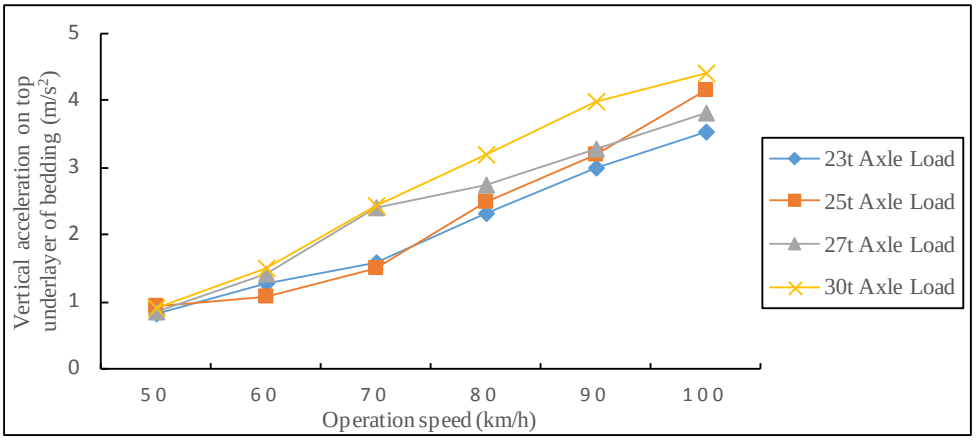

Figure 10: The vertical acceleration on top underlayer of bedding under different axle load train

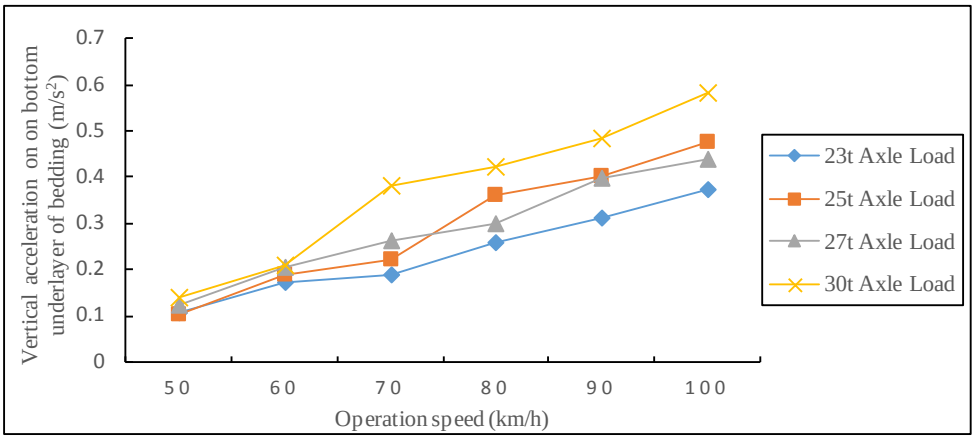

Figure 11: The vertical acceleration on bottom underlayer of bedding under different axle load train

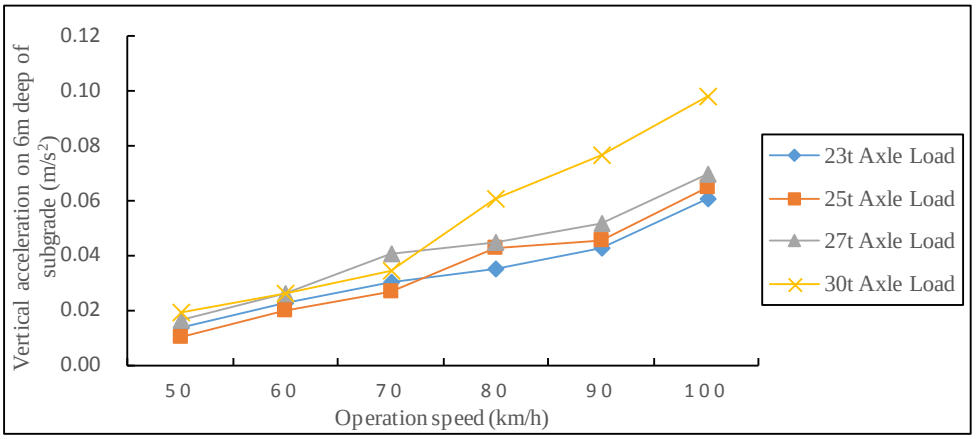

Figure 12: The vertical acceleration on 6m deep of subgrade under different axle load train

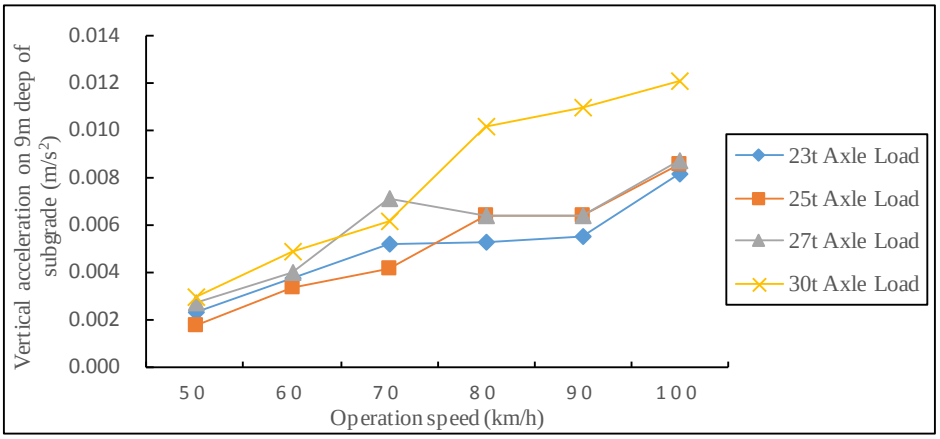

Figure 13: The vertical acceleration on 9m deep of subgrade under different axle load train

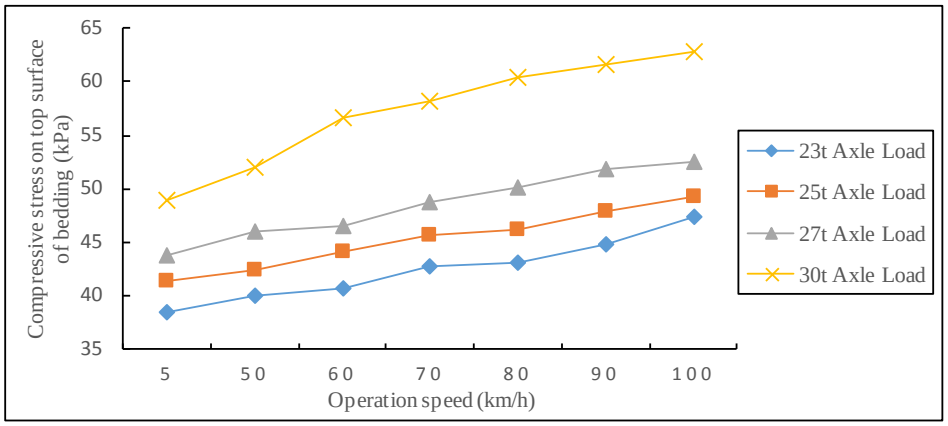

Figure 14: The dynamic stress on top surface of bedding under different axle load train

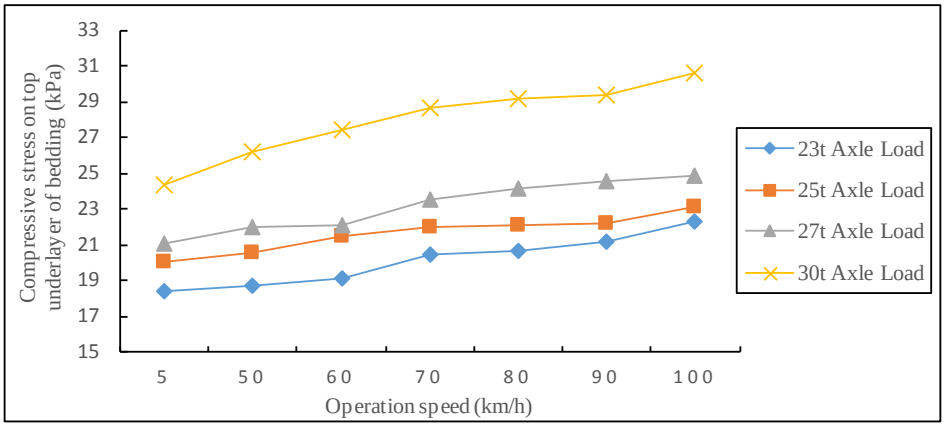

Figure 15: The dynamic stress on top underlayer of bedding under different axle load train

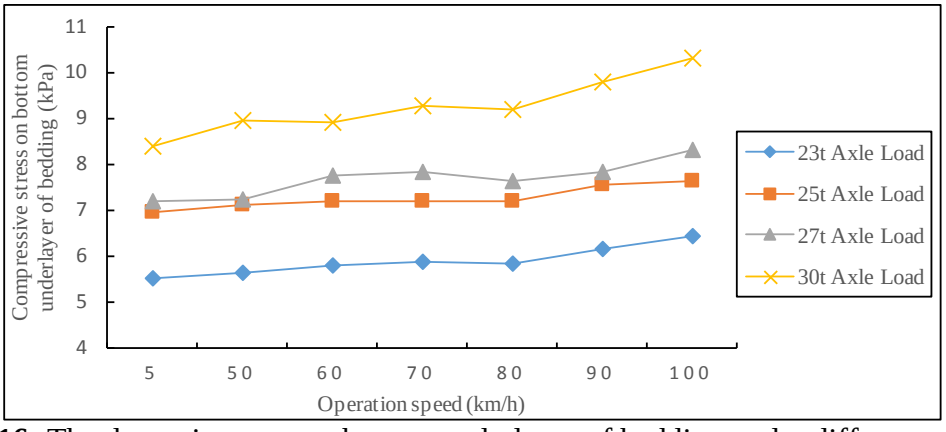

Figure 16: The dynamic stress on bottom underlayer of bedding under different axle load train

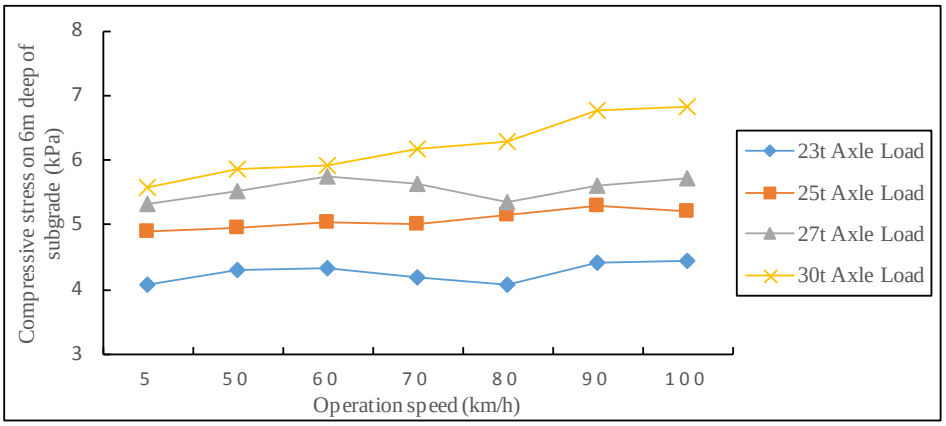

Figure 17: The dynamic stress on 6m deep of subgrade under different axle load train

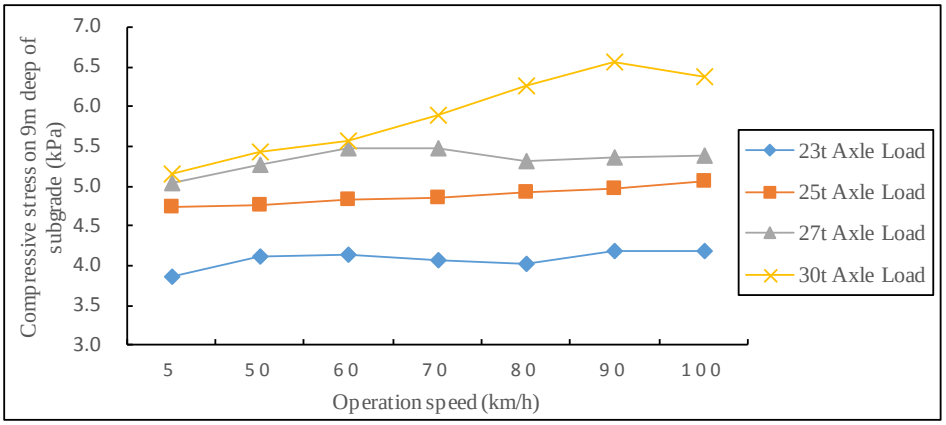

Figure 18: The dynamic stress on 9m deep of subgrade under different axle load train

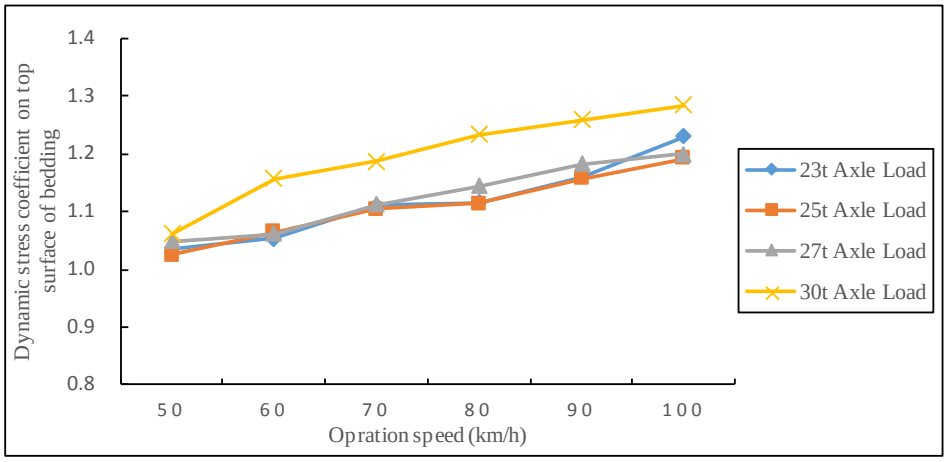

Figure 19: The dynamic stress coefficient on top surface of bedding

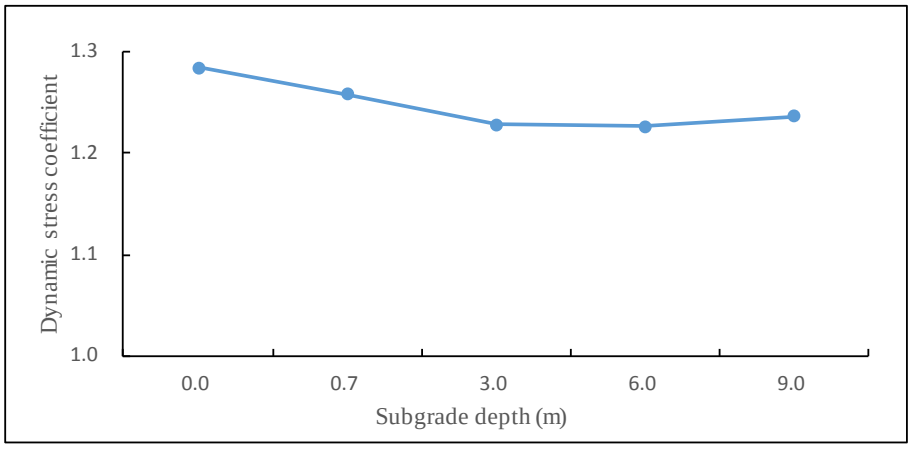

Figure 20: The dynamic stress coefficient on different depth (30t axle load, v=100km/h)

CONCLUSION

In this paper, the heavy haul train-track-subgrade dynamic coupling model is established and the dynamic response characteristics of subgrade under different axle load train at different speed has been analyzed and the following conclusions can be drawn:

(1) The dynamic response time-history curve of each layer of subgrade can be obtained clearly by using the heavy haul train-track-subgrade dynamic coupling model.

(2) The dynamic stress and acceleration of subgrade decay with depth and the decay rates of acceleration and dynamic stress in the surface of bedding were the fastest (the decay shows 52% and 43% respectively), followed by the underlayer of bedding and subgrade.

(3) The vibration acceleration of subgrade increases with the axle load and train speed but the increase amplitude decreases with the depth. When the train speed is more than 90km/h, the effects of axle load and the per-meter quality on the vertical acceleration of underlayer bedding area should be considered together.

(4) The dynamic stress of subgrade increases with the axle load and train speed. Under the same axle load train, the dynamic stress of subgrade decreases with the subgrade depth.

(5) The dynamic stress coefficient of subgrade increases with the growth of train speed. We recommend that the value of dynamic stress coefficient is 1.3 when the train speed below 100km/h.

ACKNOWLEDGMENTS

The research described in this paper was financially supported by the Science and Technology Foundation of China Railway Corporation (Grant No. SY2016G001); the Joint Fund of the National Natural Science Foundation of China (Grant No. U1361204); the National Natural Science Foundation of China (Grant No. 51378513); the Science and Technology Foundation of China Railway 14th Bureau Corporation Limited (Grant No. 20160016).

REFERENCES

1. Fujikake T. A Prediction Method for the Propagation of Ground Vibration from Railway Trains[J]. Journal of Sound and Vibration, 1986, 111(2): 357-360.
2. Kaynia A, Madshus C, Zackrisson P. Ground Vibration from High Speed Trains: Prediction and Countermeasure [J]. Journal of Geotechnical and Geoenvironmental Engineering, Proceedings of the ASCE, 2000, 126(6): 531-537.
3. Hirokazu Takemity, Shuhei Satonaka and Xie Weiping. Train Track-Ground Dynamics Due to High Speed Moving Source and Ground Vibration Transmission[J]. Structural Eng/Earthquake Eng, JSCE, 2001, 18(2): 299-309.
4. Kim, Seong Min. Vibration and Stability of Axial Loaded Beams on Elastic Foundation under Moving Harmonic Loads[J]. *Engineering Structures*, 2004, 26(1): 95-105.
5. Takemiya H. Substructure Simulation of Inhomogeneous Track and Layered Ground Dynamic Interaction under Train Passage[J]. *Journal of Engineering Mechanics*, 2005, 131(7): 699-711.
6. Cui F, Chew C H. The Effectiveness of Floating Slab Track System [J]. *Receptance methods Applied Acoustics*, 2000, (61): 441-453.
7. Diehl R J, Nowack R, Holzl G. Solutions for Acoustical Problems with Ballastless Track [J]. *Journal of Sound and Vibration*, 2002, 31(3): 899-906.
8. Xin Tao, Gao Liang. Reducing Slab Track Vibration into Bridge using Elastic Materials in High Speed Railway [J]. *Journal of Sound and Vibration*, 2011, 11(23): 2237-2248.
9. Zeng Zhiping, Liu Fushan, Yu Zhiwu, Lou ping, Zhao Yangang, Peng Limin. Formulation of Three-Dimensional Equations of Motion for Train–Slab Track–Bridge Interaction System and its Application to Random Vibration Analysis [J]. *Applied Mathematical Modelling*, 2016, 40(11-12): 5891-5929.
10. Zhai Wanming, Xia He, Cai Chengbiao. High-Speed Train–Track–Bridge Dynamic Interactions-PartII[J]: Experimental Validation and Engineering Application[J]. *International Journal of Rail Transportation*, 2013, 1(1): 25-41.
11. Wei Wei, Zeng Zhiping, Xie hong, Huang Zhihe, Song Shanyi. Hydrodynamic Pressure of the Interface Bond Damage between the CRTSIII Slab Track and Self-Compacting Concrete[J]. *Electronic Journal of Geotechnical Engineering*, 2016, 21: 5999-6011.
12. Oscarsson J, Dahlberg T. Dynamic Train/Track Ballast Interaction Computer Models and Full-Scale Experiments[J]. *Vehicle System Dynamics*, 1998, 28(Suppl): 73-84.
13. Auersch L. Vehicle-track Interaction and Soil Dynamics[J]. *Vehicle System Dynamics*, 1998, 28(Suppl): 553-558.
14. Yu Zhiwu, Mao Jianfeng, Guo Fengqi, et al. Non-Stationary Random Vibration Analysis of a 3D Train-Bridge System using the Probability Density Evolution Method[J]. *Journal of Sound and Vibration*, 2016, 366(3): 173-189.
15. Mao Jianfeng, Yu Zhiwu, Xiao Yuanjie, et al. Random Dynamic Analysis of a Train-Bridge Coupled System Involving Random System Parameters Based on Probability Density Evolution Method[J]. *Probability Engineering Mechanics*, 2016, 46(10): 48-61.

16. Lei, X., Noda, N.A. Analyses of Dynamics Response of Vehicle Track Coupling System with Random Irregularity of Track Vertical Profile[J]. *Journal of Sound and Vibration*, 2002, 258(1): 147-165.

17. Sato, Y. Study on High-Frequency Vibrations in Track Operated with High-Speed Trains[J]. Quarterly Reports of Railway Technical Research Institute, 1997, 18(3): 109-114.

Editor's note.
This paper may be referred to, in other articles, as:

Wei Wei, Zeng Zhi-ping, Wu Bin, Wang Wei-dong, and Yan Hai-jian: "Dynamic Characteristics of Railway Subgrade under Heavy Haul Train" *Electronic Journal of Geotechnical Engineering*, 2017 (22.01), pp 209-232. Available at ejge.com.